

## Ion heating near the ion composition boundary at Venus

### Authors:

K. Szego <sup>(1)</sup>  
Z. Dobe <sup>(2)</sup>  
Z. Bebesi <sup>(1)</sup>  
L. Foldy <sup>(1)</sup>  
M. Fraenz <sup>(3)</sup>  
A. Opitz <sup>(1)</sup>

### Affiliations:

<sup>(1)</sup> Wigner Research Centre for Physics, Budapest, Hungary  
<sup>(2)</sup> General Electric Company, Budapest, Hungary  
<sup>(3)</sup> Max-Planck-Institut für Sonnensystemforschung, 37077 Göttingen, Germany

### Correspondence E-mails:

K. Szego:  
[szego.karoly@wigner.mta.hu](mailto:szego.karoly@wigner.mta.hu)  
Z. Dobe:  
[zoltan.dobe@ge.com](mailto:zoltan.dobe@ge.com)  
Z. Bebesi:  
[bebesi.zsofia@wigner.mta.hu](mailto:bebesi.zsofia@wigner.mta.hu)  
L. Foldy:  
[foldy.lajos@wigner.mta.hu](mailto:foldy.lajos@wigner.mta.hu)  
M. Fraenz:  
[fraenz@mps.mpg.de](mailto:fraenz@mps.mpg.de)  
A. Opitz:  
[opitz.andrea@wigner.mta.hu](mailto:opitz.andrea@wigner.mta.hu)

### Abstract

In this study, we focus on plasma processes in the boundary layer above the ionopause of Venus. The first measurements which demonstrated the existence of such a boundary layer were those of the electron energy spectra obtained by the Pioneer Venus Orbiter Retarding Potential Analyser (ORPA). The measurements of the ASPERA-4 electron spectrometer on board the Venus Express (VEX) confirmed the existence of such a layer. The upper end of the interaction layer, where planetary ions disappear, is called ion composition boundary (ICB). Due to the interaction of the two plasma populations near the ICB – the shocked solar wind and planetary ions – instabilities are excited. The instabilities also heat the ions. Using the 3-D energy and spatial coverage of the Analyser of Space Plasmas and Energetic Atoms (ASPERA-4) instrument suite on board VEX, we compare here with the data the charged particle heating due to the modified two stream instability (MTSI) model. We show that MTSI heating is effective up to a few hundred eV. We also discuss the limits of this approach.

## 1. Introduction

The plasmasphere of Venus is possibly the best explored in our Solar System except Earth. The first successful flyby to Venus was Mariner-2 on 14 December 1962, followed by many more missions opening the detailed study phase which was then crowned by Pioneer Venus Orbiter (PVO), and by the Venus Express Mission (VEX). PVO entered orbit on 4 December 1978, and was operational till 22 October 1992. The orbit plane of the Pioneer Venus spacecraft was nearly polar (with a periapsis at  $17^\circ$  N latitude at arrival, and moved to  $10^\circ$  S during the mission); the spacecraft was spinning with its spin axis normal to the plane of the Venus orbit. PVO operated very successfully, and in certain sense it significantly contributed establishing planetary space plasma physics. We refer here to the special PVO issue of *Journal of Geophysical Research* [December 1980] and to *Vol. 55 of Space Science Review* [1991] on Venus Aeronomy, edited by C.T. Russell.

The Venus Express (VEX) mission, recently exploring Venus, was launched on 9 November 2005, and arrived at Venus on 11 April 2006. After eight years in orbit, ESA's Venus Express completed an aerobreaking manoeuvre and the mission was finished in the planet's hostile atmosphere in 2015. Its operational orbit around Venus was a 24-hour elliptical, quasi-polar orbit (the latitude of the pericenter is at  $\sim 76^\circ$  North relative to Venus orbit). At its closest to Venus, VEX reached an altitude of 250 kilometers and at its furthest, it was 66 000 kilometers away from the planet. Between 13 July and 4 August 2009 a series of manoeuvres further lowered the pericenter of the orbit into the range 185-300 km. The orbit was inertially fixed

In this study, we focus on the boundary layer above the ionopause of Venus. We summarize first the relevant PVO then the VEX observations. The first

measurements which demonstrated the existence of such a boundary layer were those of the electron energy spectra obtained by the Pioneer Venus Orbiter Retarding Potential Analyzer (ORPA) (1). The characteristics of the electron spectra observed by ORPA above the ionopause were different from both those observed inside the ionosphere and those of the shocked solar wind, and shared the signatures of the two. The region was termed as "mantle" by the authors. The width of this region was found to depend strongly on the solar zenith angle; along the Sun-Venus line it was of the order of 100 km. The measurements of the ASPERA-4 electron spectrometer onboard Venus Express (VEX) confirmed the existence of such a layer, c.f. Figure 2 in (2). Further measurements proved that the plasma region between the ionopause and the bow shock is structured. In (3) it was shown that the bulk of the shocked solar wind protons are deflected above the ionopause while the total magnetic field increases and a magnetic barrier is formed (3); it is a layer extending from the peak  $B_{\text{total}}$  value up to the altitude where the magnetic pressure is half of the solar wind ram pressure (corrected by barrier normal angle).

PVO carried onboard an electric field detector that measured waves in four channels centered on 100 Hz, 730 Hz, 5.4 kHz, and 30 kHz. The analysis of all relevant PVO data has confirmed that the most intense waves on the dayside were detected in the 100-Hz channel above the peak of the magnetic barrier, in the interaction region (4). Most probably, the waves are excited by the mixed plasma population present in this region (5).

On board PVO the orbiter's ion mass spectrometer (OIMS) was capable of measuring suprathermal ions in the 30 to 75 eV energy range (though they could not be distinguished from protons accelerated to

75-90 eV); see Figure 3 in (6). It was concluded that such ions on the dayside were predominantly seen in the ionopause region extending from 7 to 18 local hours, the measurements had a sharp boundary at low altitudes.

The Orbiter Plasma Analyzer (OPA) was primarily designed for solar wind monitoring with a low time resolution of about 10 min (7). OPA was a quadrispherical electrostatic analyzer; the energy/charge range was 50–8000 eV/q (ions) in 32 steps and 1–500 eV (electrons) in 16 steps. The angular range covered was  $\pm 85^\circ$  elevation. However, due to the low time resolution there are no characteristic data inside the interaction layer we are interested in. The upper end of the interaction layer, where planetary ions disappear, is called ion composition boundary. Our current knowledge about the structure of this layer was established by the ASPERA-4 sensor suite on board of Venus Express (8). In (9), analysing the ASPERA-4 charged particle data has come to the conclusion that there is an “ion composition boundary (ICB)” between the IP and the BS that separates the shocked solar wind from the planetary ions. The analogue boundary at Mars was discovered by Lundin et al. (10) using the data of the ASPERA instrument on board of Phobos-2 spacecraft, and termed it the Mass Loading Boundary (MLB). The investigators suggested that the magnetosphere of Mars is contained in an exterior composition boundary, the MLB, and an interior boundary, the magnetopause. The induced magnetospheres of Venus, Mars, and Titan were reviewed in details in (11). As pointed out, the outer boundary of the induced magnetosphere is characterized by an enhancement of magnetic field draping and massloading, along with a change in the plasma composition, a decrease in the plasma temperature, a deflection of the external flow. These features are not necessarily co-located. The MLB of Lundin

et al. (10) and the ICB discussed here are practically identical.

The boundary layer plays a special role in the ion escape from Venus (12); their investigation has led to interesting results concerning the ion structure of the tail. From the period 24 May 2006 to 12 December 2007, the investigators selected 114 orbits suitable for the study. It was concluded that the ions escape occurs through two well distinguished regions behind the terminator, the central part of the plasma wake, the plasma sheet, and a circular area close to the induced magnetosphere boundary separating the solar wind void from the shocked solar wind plasma. They have also obtained velocity vectors for the different ion components in the tail, exhibited in Figure 6 of that paper. The velocity vectors are highly irregular near the planet. Such irregularity is indeed a signature of turbulent plasma flow near the planet. Their analysis show that ions can flow backwards, towards Venus. Plasma turbulence in the tail was confirmed in (10), reporting the existence of a large-scale ion flow vortex, a curled tailward flow of SW protons and ionospheric  $O^+$  in the Venus plasma tail. We need to bear in mind this turbulent structure of the tail in the subsequent analysis.

Solar wind forcing of the ion outflow, that is the effect of electric field due to the solar wind acting on planetary ions has an important role in ion escape both at Venus and Mars. Ion acceleration and heating associated with the outflow and escape of ionospheric ions from Mars and Venus was discussed in reviews in (10, 13); see further references there. The latter paper gives an overview of the physical processes relevant for the different main escape channels (e.g. polar wind, plasma sheet, ion pick-up, escape through auroral flux tubes, etc.) including the boundary layer, a region where the momentum lost by the solar wind is coupled to the planetary plasma. Coupling

might be the result of magnetic field stresses, and anomalous plasma transport processes.

Solar wind entering the boundary layer is decelerated by the  $\mathbf{j} \times \mathbf{B}$  forces at the magnetic barrier. Since ions are not magnetized on such scales, only polarization electric field is effective. Gradual deceleration of the solar wind ions takes place in the boundary layers while entering the magnetic barrier with outward pointing electric field; whereas local planetary plasma gain energy when crossing this potential drop. Ion populations moving with different velocities with respect to the net center of charge experience different electric fields (13). The interface between the magnetosheath and ionospheric plasmas is also a site for possible fluid-like MHD instabilities; they may lead to detached plasma structures. Another probable mechanism for collisionless momentum coupling between interpenetrating plasmas in the boundary layers could be plasma instabilities driven by the relative motion of ions and electrons, this will be dealt with in Section 3.

In this study we focus on the plasma region near the ICB. Due to the interaction of the two plasma populations near the ICB – shocked solar wind and planetary ions – instabilities might be excited. This will be discussed in Section 3, together with the possible observable effects. In the early analyses of the instabilities the possible excited waves were studied; in this study we model the effect of the instabilities on the ion populations in Section 4.

## 2. Data analysis

For our analysis we use the proton,  $O^+$  and electron energy spectra of the VEX ASPERA-4 sensor suite, these data are complemented by the VEX magnetic field measurements (14).

The ASPERA-4 (15) comprises an Ion Mass Analyser (IMA), it provides ion measurements in the energy range 0.01–36 keV/q for the main ion components with  $M/q > 40$  amu/q. Its energy resolution is  $\Delta E/E = 0.06$ , the field of view (FOV) is  $90^\circ \times 360^\circ$ , the angular resolution is  $10^\circ \times 22.5^\circ$ ; and the time resolution for a full 3-D data acquisition is 192 s. The IMA FOV sensor can be modeled as a cylinder; its axis is the direction about which the FOV is  $360^\circ$ , and the height of the cylinder for lines starting from the cylinder centre models the  $\pm 45^\circ$  FOV in the perpendicular direction. However, owing to location of IMA on the spacecraft, the spacecraft body and the solar panels partially obscure the full FOV (see e.g. Figure 3 in (12)). The electron sensor (ELS) is an axially symmetric quadrispherical analyzer; for the observations shown ELS covered the spectral range from 0.8 eV to 30 keV, electron spectra were measured about every 4 s. The ASPERA-4 sensor is unique relative to all previous instruments flown around Venus because it measures 3D plasma distributions above 10 eV, making possible to derive the moments of the major ion components, for the first time since the exploration of Venus started. Due to the high 3D velocity resolution of ASPERA-4 the time resolution is relatively low, and accordingly the spatial resolution is low as well. Despite, ASPERA-4 goes much beyond PVO capabilities.

In (9) the positions of the Venusian BS and ICB was determined at solar minimum based on ASPERA-4 observations made on board VEX. The BS was identified by an increase in density of energetic electrons in the magnetosheath with respect to the solar wind because electrons were measured with higher resolution than ions, leading to a more accurate determination of the boundary location. The ICB separates the cold plasma of the ionosphere from the hot magnetized plasma of the magnetosheath. It was

identified by the vanishing of solar wind protons and the appearance of planetary ions. Here we use the same technique to find out plasma properties in the vicinity of the ICB.

We have analysed visually all planetary ion spectra measured by ASPERA-4 from the beginning of the mission till the end of 2012 with the help of the tools provided by AMDA system [<http://amda.cdpp.eu/>]. Though such a survey is prone to biases, the result is that in about 30-40% of the cases (depending on how we set the energy limit) the spectra show heated planetary ions at the ICB, in one 192-s long spectrum-line (with a few exceptions); sort of burst like heating. A part of the study is to investigate to which extent the proposed MTSI instability can explain the observed heating. To understand this in depth, we selected two cases (one slow and low density case, and one high speed and high density case) discussed below.

Fig. 1 and 2 exhibit data taken on 3 Dec. 2008, and 5 Nov. 2011, respectively. Data in Figure 1 shows more or less average plasma conditions, the events in Figure 2 were collected when a solar storm was hitting Venus. The top panels in Figure 1 and 2 exhibit the spacecraft orbit in a cylindrical coordinate system, time is also shown, the dots delimit 10 min long time interval. The two continuous blue lines are the nominal BS and ICB locations. In Figure 1 and 2 in the three middle panels charged particle spectra are presented as measured by ASPERA-4, namely solar wind protons, planetary  $O^+$  ions, and electrons; the plots exhibit counts in the different energy ranges, the number of counts is colour coded. In the two bottom plots the total magnetic field (in 10s resolution) and the spacecraft altitude above the planetary surface is shown; all for a one-hour long time period around the ICB

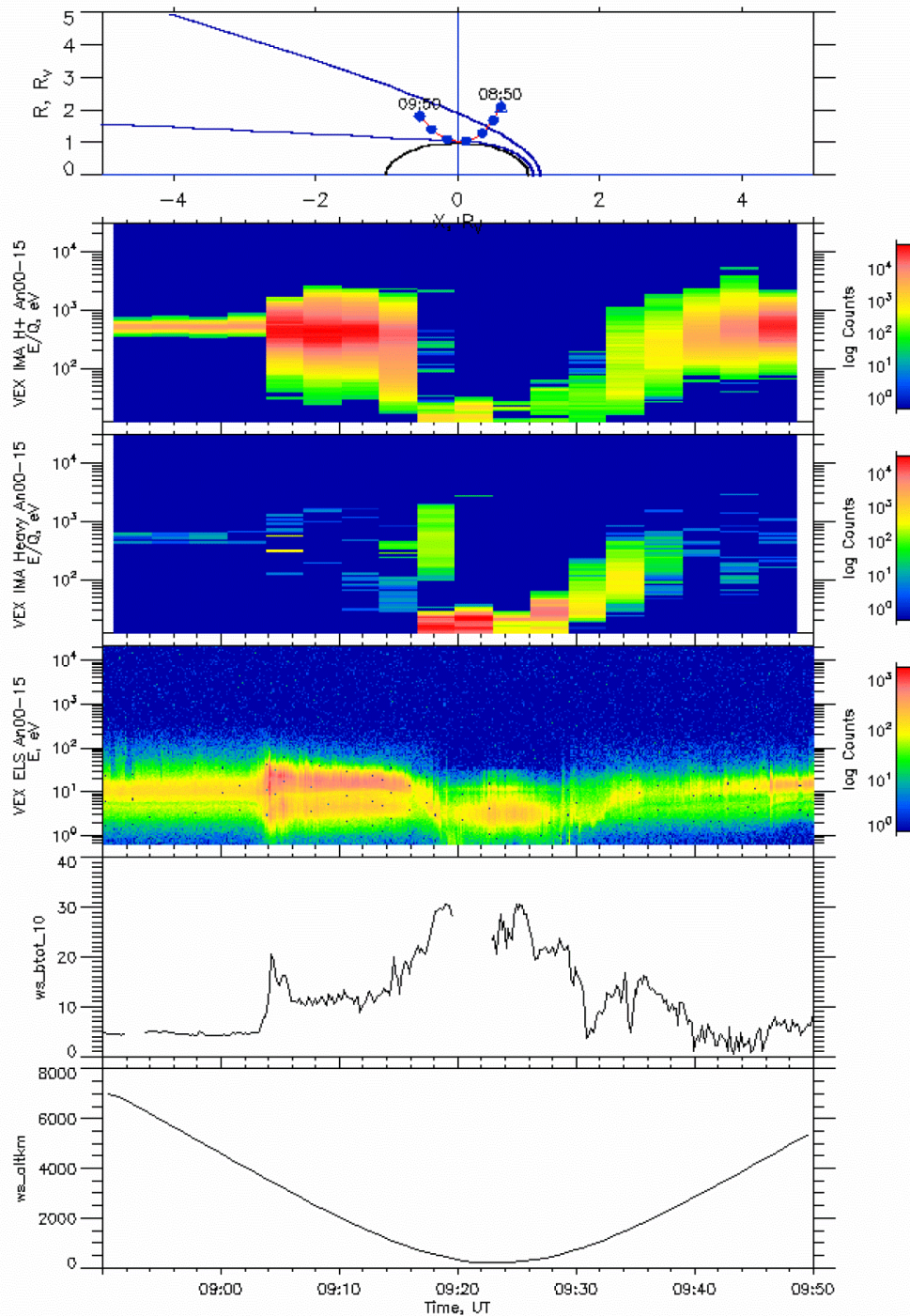
In Figure 1 data for 2008.12.03 are shown. The flow of events starts inbound in

the solar wind at 8:50; the BS was crossed near 9:04 as shown by the magnetic field data. The frequently sampled electrons are heated at the same time; the change of the proton spectra despite the 192s long measurement time interval appears at the same time. The next three proton spectra were taken in the sheath, no  $O^+$  ions were present. At 9:16 all spectra indicate that we reached the ICB, at about 9:18 the spacecraft crossed the ionopause according to the magnetic field and electron data.

In Figure 2 data for 2011.11.05 are shown. The flow of events starts inbound in the solar wind at 6:40; the BS was crossed near 7:00 as shown by the magnetic field data. The frequently sampled electrons are heated at the same time; the change of the proton spectra due to the 192s long measurement time interval appears already sooner. The next two proton spectra were taken in the sheath, no  $O^+$  ions were present. At 7:09 all spectra indicate that we reached the ICB, at about 7:12 the spacecraft crossed the ionopause. On both figures the formation of the magnetic barrier is clearly seen.

On 3 Dec. 2008 the solar wind approached Venus with  $v_{sw} \sim 230$  km/s,  $n_p \sim 0.6$ /cc,  $T_{sw} \sim 4$  eV; behind the bow shock in the sheath it slows down to 120 km/s, the density jumps to 50/cc and the flow was heated to  $\sim 15$  eV. The peak magnetic field reached  $\sim 30$ nT. The spacecraft crossed the ICB at about 09:16 UT. However, we note that the moments are classified as “poor quality” due to the visibility constraints.

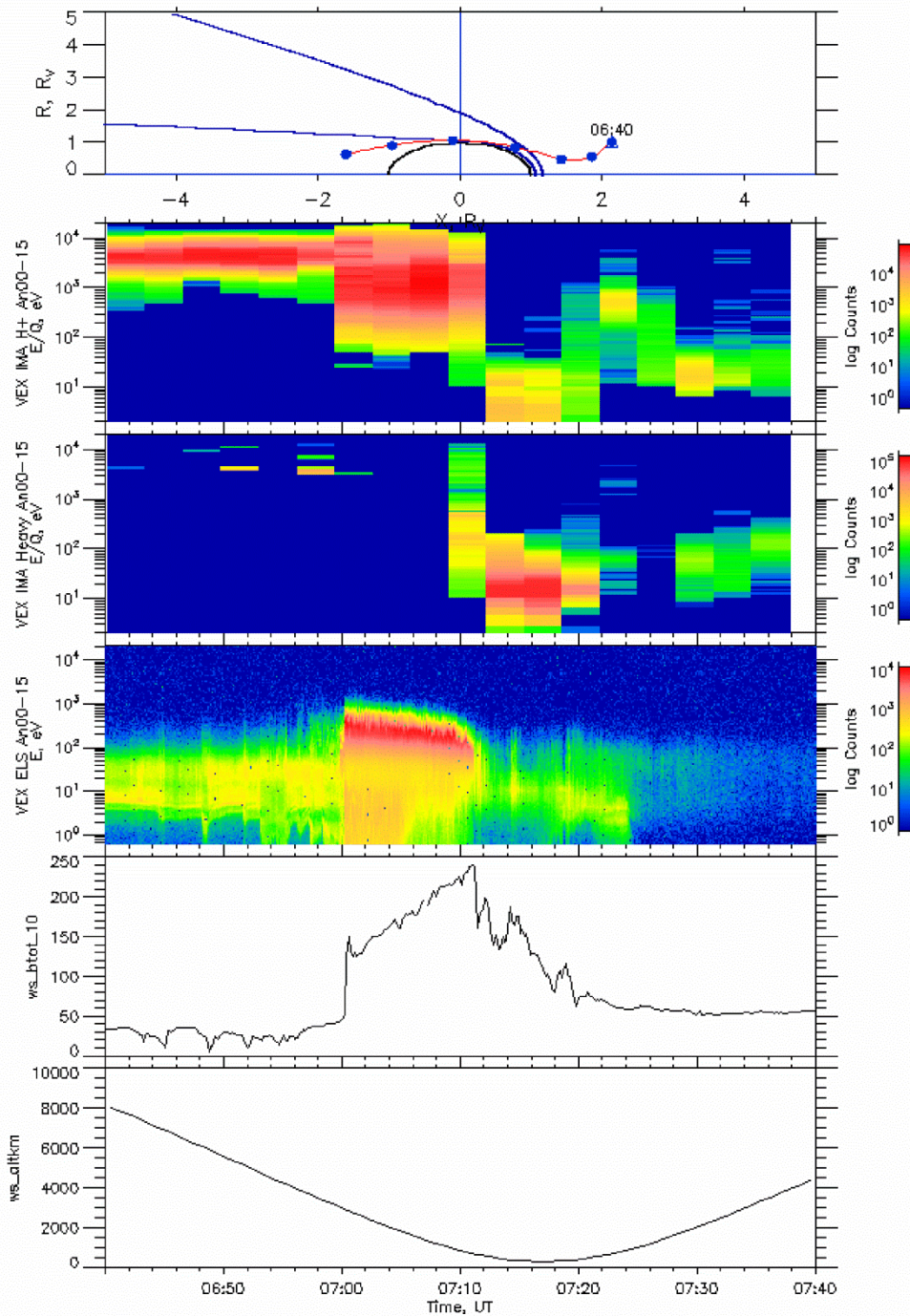
On 5 Nov. 2011 a solar CME approached Venus with  $v_{sw} \sim 880$  km/s,  $n_p \sim 10$ /cc,  $T_{sw} \sim 70$  eV; behind the bow shock in the sheath it slows down to  $\sim 200$  km/s, the density jumps to 100/cc and the flow was heated to  $\sim 100$  eV. The peak magnetic field reached  $\sim 300$ nT. The spacecraft crossed the ICB at about 07:10 UT.



Dec 3 2008

Created by AMDA(C) 2.0 Sat Dec 28 13:10:20 2013

**Figure 1.** The top panels (for data measured between 2008-12-03T08:50 - 09:50) exhibit the spacecraft orbit in a cylindrical coordinate system, time is also shown, the dots delimit 10 min long time interval. The two continuous blue lines are the nominal BS and ICB locations. In the three middle panels we present charged particle spectra measured by ASPERA-4, namely electrons, solar wind protons and planetary  $O^+$  ions; the plots exhibit counts in the different energy ranges, the number of counts is colour coded. In the two bottom plots the total magnetic field (in 10s resolution) and the spacecraft altitude above the planetary surface is shown; all for a one-hour long time period around the ICB.



Nov 5 2011

Created by AMDA(C) 2.0 Sat Dec 28 08:30:31 2013

**Figure 2.** Same as Figure 1 for data measured between 2011-11-05T06:40 – 07:40.

It can be seen in both figures that planetary ions are significantly energized near ICB; this is a general feature present in a significant portion of similar flyby ion data, as mentioned above. It was established

by ASPERA-4 measurements (see e.g. (12, 15)) that the near-ICB region is one of the locations of plasma escape. Ion energization might occur due to pickup, (see e.g. Figure 1 in (15)), in Figure 1 and 2 no similar pickup

events could be identified. It was also pointed out that instabilities excited near the ICB energize planetary ions and may lead to the generation of detaching ion clouds (16).

In this study, we present a numerical hybrid code model, described in detail in the next section that leads to ion energization near ICB/IP via modified two-stream instability. It was suggested in (5) that the ions seen in (6) are these energized ions near ICB/IP; and this instability excites the 100-Hz waves observed by the plasma wave instruments flown on PVO (see e.g. (17)).

### 3. Beam-driven instabilities at Venus

It has been well established that on the dayside of Venus plasma waves are excited, and the most intense waves were observed in the 100-Hz channel of the orbiter electric field detector (18), with typical average amplitudes around tens of mV/m (17) and references therein. The modified two stream instability (MTSI) (19) and the ion acoustic current driven instability (20) have both been suggested as explanations. In (21) Szego et al. analysed the robustness of the ion acoustic scenario and showed that the presence of even a small amount of cold planetary electrons quenches the ion acoustic mode.

Significant collisionless momentum and energy exchange takes place in this transition region between ICB and IP because of wave-particle interaction, creating a highly turbulent layer, where the bulk properties of the plasma significantly changes. (This mechanism is also called “anomalous viscosity” in (19)).

Two types of instability modes were proposed as explanations of the observed wave activity in the Venus and Mars plasma mantle: the lower hybrid drift and modified two-stream instability (MTSI) with typical frequencies in the vicinity of the lower hybrid frequency and wavelength of the

order of solar wind electron gyroradius (21, 5, 22, 23); and a beam resonant instability branch of ion acoustic type waves (20) with frequencies of the order of ionospheric ion plasma frequency, and typical wavelength of order of electron Debye length. In (24) Szego et al. analysed the robustness of the ion acoustic scenario and showed that the presence of even a small amount of cold planetary electrons quenches this mode.

Dobe and Szego in (25) performed a parametric study within the framework of the linear Vlasov theory of the instability modes viable within the flowside plasma mantle of Titan. Although these calculations were performed for conditions within the flowside plasma mantle of Titan it can be shown that the main conclusions are valid for the solar wind-ionosphere interaction region of Venus and Mars as well. According to this study the fastest growing plasma waves possibly excited within the flowside plasma mantle of Titan correspond to “lower hybrid” and the ion acoustic type modes generated by modified two-stream instabilities [see, e.g., (26, 5) and ion-ion acoustic beam instabilities [see, e.g., (27)], respectively. The modified two-stream instability modes have frequencies and growth rates in the lower hybrid frequency range with wavelength between the electron and the ion gyroradius and propagate nearly perpendicular to the magnetic field. The ion-ion acoustic instability is a shorter wavelength (order of hot proton Debye length) and higher-frequency (order of ion plasma frequency) electrostatic mode. It was also shown that the ion acoustic mode smoothly transforms into the lower hybrid mode when the relative number density ratio of cold electrons becomes comparable to or less than  $10^{-2}$ . This means that the two dominant instability types can only exclusively be present in well separated spatial regions determined by the presence/absence of cold ionospheric electrons.

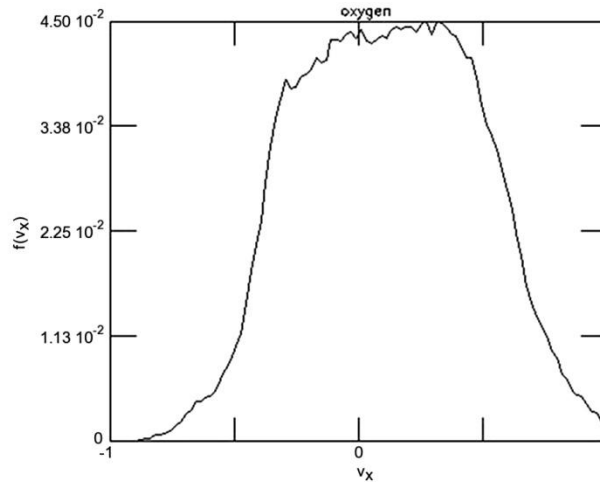


**Figure 3a.** Simulated heavy ion phase space distribution for the 2008 case. The horizontal axis displays velocity normalized to proton thermal velocity.

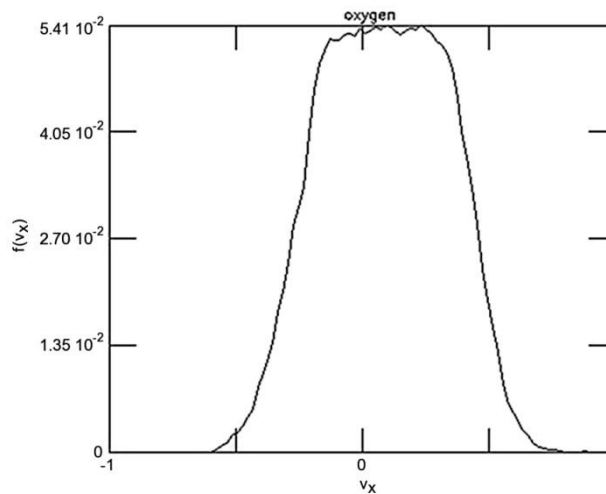


**Figure 3b** Same as Figure 3a for the 2011 case.

The first PIC-type simulation of the plasma wave generation within the interaction region of nonmagnetic planets with substantial atmosphere such as Mars and Venus was given by Quest et al. (27), where the bulk velocity of the streaming plasma was constricted to direction strictly perpendicular to the ambient interplanetary magnetic field. This model was further developed by Dobe et al. (23) allowing for arbitrary though fixed wave propagation direction with respect to the external magnetic field lines. More recently Dobe et al. (28) extended the investigation for the case of interaction of Titan's ionosphere with the streaming plasma of Saturnian magnetosphere or solar wind origin. These

models intended to give a “local” rather than “global” description of the microphysics taking place during the interaction of the hot streaming plasma environment (of either magnetospheric or solar wind origin) with the cold ions of planetary origin. In order to describe phenomena such as lower hybrid type wave generation and nonlinear wave particle interaction involving realistic electron inertia the characteristic spatial resolution was needed to be reduced to the order of few electron thermal gyroradii. Using the same resolution in a 3-D global hybrid simulation model (such as presented in (29,30,31)) would need extremely large CPU time even on today's supercomputer power.

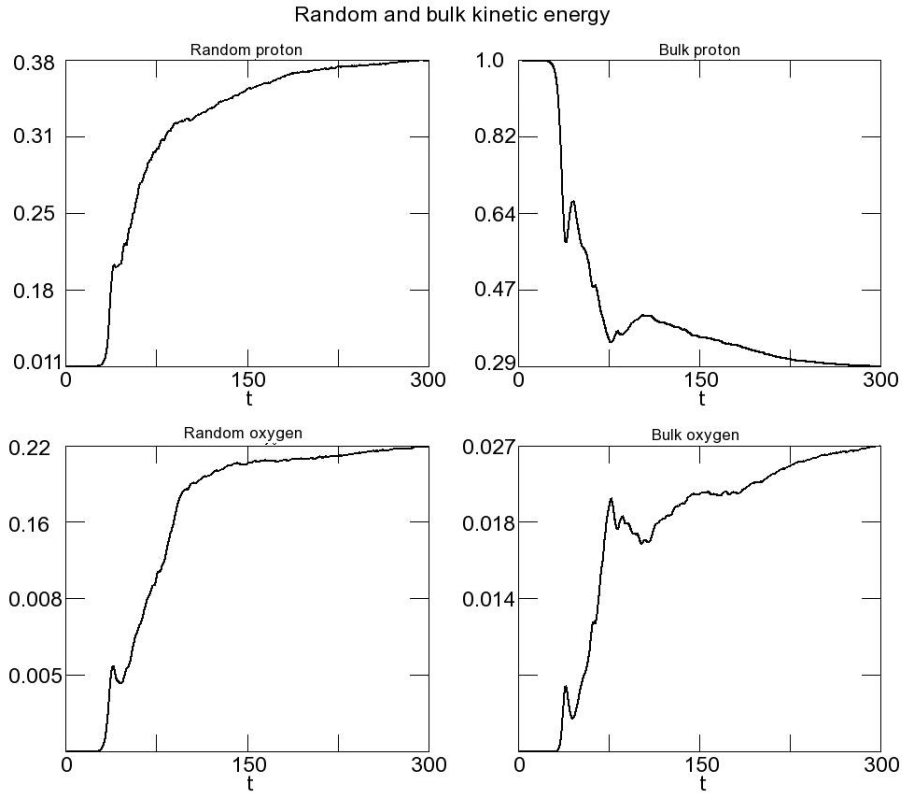


**Figure 4a.** Simulated bulk and random energy of protons and oxygen ions for the 2008 case; see description in the text.

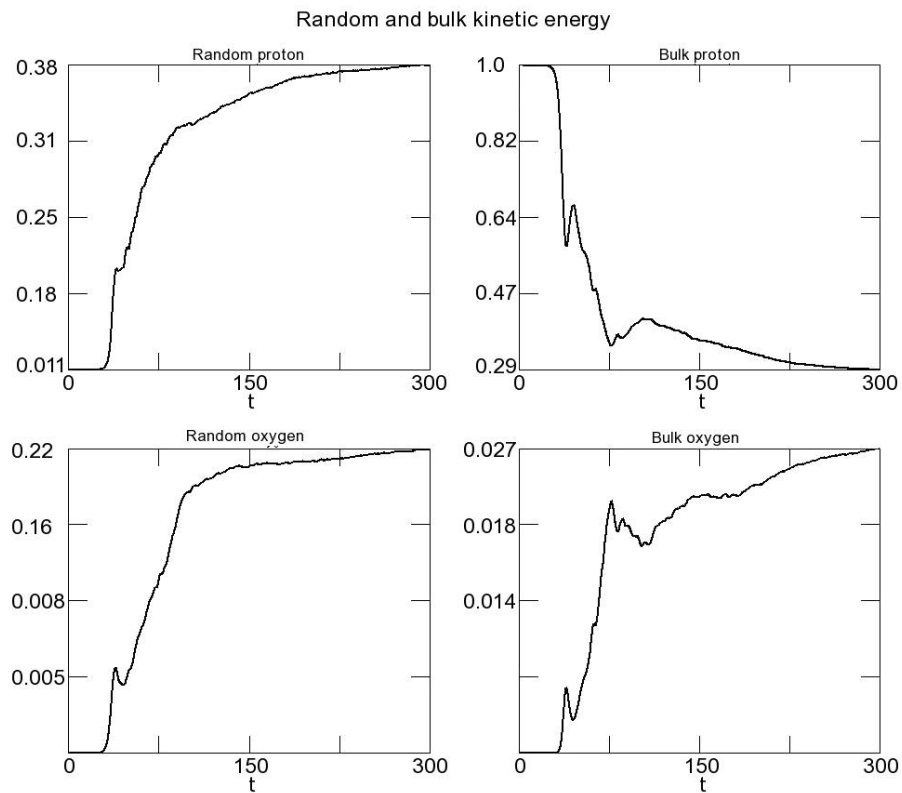


**Figure 4b.** Same as Figure 4a for the 2011 case.

Our present 1-D hybrid PIC model is capable to describe the main features of the linear and nonlinear evolution of the modified two-stream instability generated within the interaction region of Venus. Here we follow the argumentations presented by (5, 23).

In previous studies of Dobe and Szego (25) [referred later as D2005], and Dobe et al., (28) [referred later as D2007] the excitation mechanism was applied to the case of Titan. Here we present it for the Venus case.

The hot plasma flowing past Venus with drift velocity  $U_{\text{beam}}$  interacts with the cold plasma of ionospheric origin in the presence of the external magnetic field,  $B_0$ . In our model configuration we considered spatially homogeneous, Maxwellian plasma and the dispersion relation was considered for the low-frequency limit,  $\omega_{ci} \ll \omega \ll \omega_{ce}$ , assuming magnetized electrons and non-magnetized ions. The notion “unmagnetized” in this sense means that the characteristic wavelength of the instability is much smaller than the ion gyroradius and the characteristic frequency and increment of the instability is much larger than the ion gyrofrequency. Here  $\omega_{c(i,e)} = eB_0/m(i,e)c$  is the gyrofrequency of the protons (p) and (e) electrons. In (23) Dobe et al. [1999] a new, faster developing type of MTSI was proposed that better matches PVO data. For this branch of MTSI, waves are generated by

the interaction between the ionospheric oxygen ions and the cold electron beam, created by  $\mathbf{E} \times \mathbf{B}$  pickup. Electron pickup takes place over a few electron gyroperiods, a time interval much shorter than the lower hybrid period. Although the cold electron beam has a little kinetic energy of its own, the wave particle resonance is sustained for a longer time due to electron pickup under the combined action of the magnetic and convective electric field of the solar wind. This makes possible a substantial transfer of free energy from the proton flow to the waves. The excited waves are predominantly electrostatic.

The dispersion relation, following (26) is given in D2005. The instability mode driven by the relative drift between two non-magnetized ion components gives rise to the so-called lower hybrid drift instability (LHDI) waves which typically propagate in a very narrow range of angles close to directions perpendicular to the external magnetic field. More obliquely propagating waves are generated by the so-called modified two-stream instability (MTSI) scenario driven by the relative cross-field drift of non-magnetized ions and magnetized electrons. In D2005 it was shown that near the planet the MTSI mode is the dominant. The parameter dependence of the solutions was also investigated in D2005. It can be shown that the excited MTSI waves are predominantly electrostatic, i.e.,  $(\omega_{pe}/kc)/2 \ll 1$ , for the cold electron plasma beta limit.

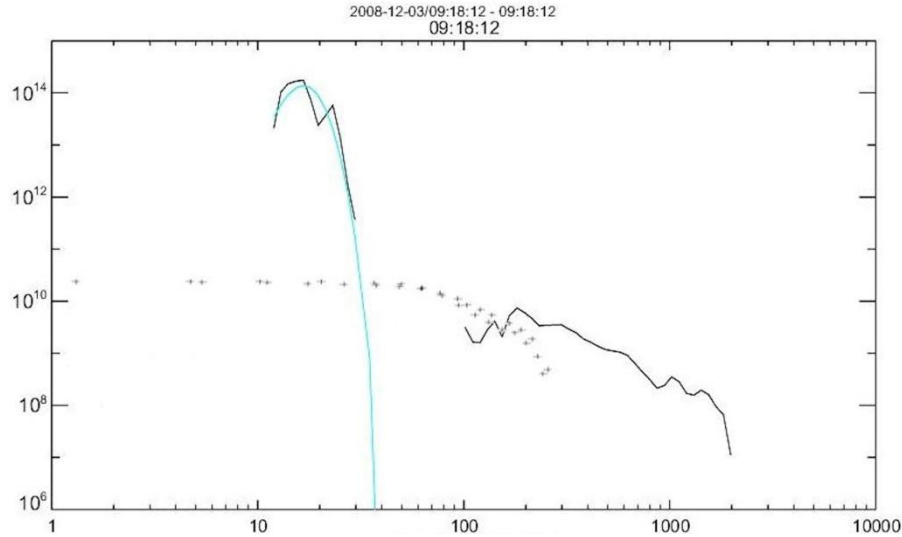


**Figure 5a.** Comparison of the measured (continuous line) and simulated (crosses) heavy ion phase space density distribution for the 2008 case. The horizontal axis is energy in eV. See further description in the text.

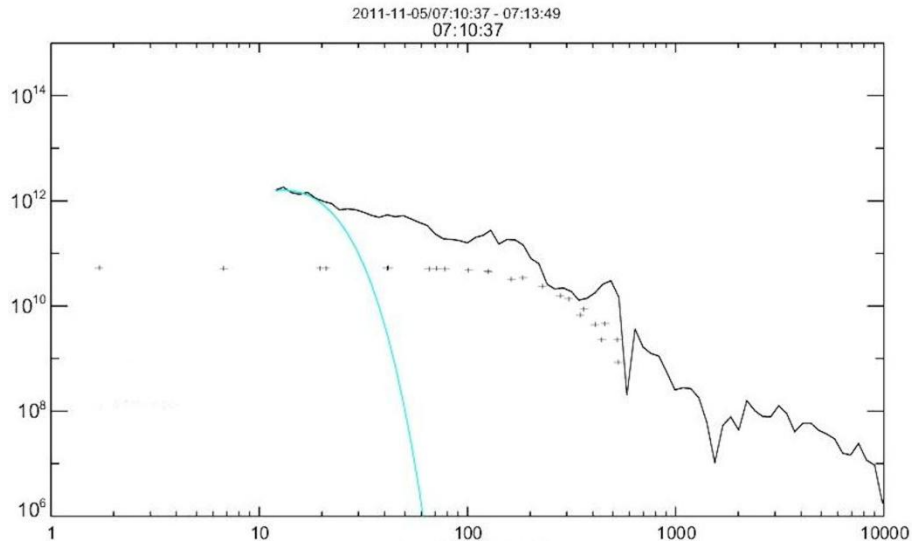


**Figure 5b.** Same as Figure 5a for the 2011 case.

A one-dimensional electromagnetic hybrid particle in-cell simulation has been constructed in order to investigate the collisionless interaction between the streaming plasma components. All the vector components retain their vector nature, but the spatial variation takes place only in one dimension along the wave propagation direction. The simulation model treats the ion species using particle-in-cell (PIC) methods. The ions approximated as macroparticles are moved using standard

time-centered leapfrog algorithms, with ion density and current collected at the corners of a rectilinear grid. Given these source terms, the electromagnetic fields are also solved on the grid, with which the ions are moved during the next time step. The field equations are solved using the predictor-corrector method described in (22). The electrons are modeled as a charge neutralizing, adiabatic fluid in which inertial and electromagnetic effects are retained. The electromagnetic field quantities are then

advanced by solving the coupled set of linear partial differential equations. In case of the electrons an isotropic pressure term is used, and the finite electron temperature is calculated by assuming an adiabatic equation of state of the form:  $T_e(x) = T_{e0}[n_e(x)/n_0]^{\gamma_e-1}$  where  $\gamma_e = 5/3$ ,  $T_{e0}$  and  $n_0$  are average initial electron temperatures and densities; according to the quasineutrality  $n_e(x)$  is equal to the local density of the ions. Using a finite pressure term is important when modelling the evolution of the MTSI. The momentum equation for the ions is solved by using the general form of the ion pressure tensor. While all vector physical quantities were kept three-dimensional, their spatial dependence was constrained to one dimension, parallel to the wave propagation direction. Periodic boundary conditions are imposed, and the initial system is allowed to relax in time. Besides the local charge neutrality another natural consequence of the one-dimensional hybrid PIC simulation model with periodic boundary conditions is the current neutrality condition (i.e., zero net electric current density in the flow direction). The particle initialization is performed by imposing relative drift between uniformly distributed Maxwellian protons and stationary ionospheric ions.

In order to describe phenomena such as lower hybrid type wave generation and nonlinear wave particle interaction involving realistic electron inertia the characteristic spatial resolution was needed to be reduced to the order of few electron thermal gyroradii. Due to that this model gives sort of a local description extending to a relatively short distance. (Distance along  $x$  is normalized to  $r^* = (v_{Tp}/\omega_{ce})$ ) This „local” nature is reflected in the one-dimensionality of the model, since it would be impossible to set boundary conditions perpendicular to the wave propagation direction. In D2007 it was shown that the model solution matches reasonable well with the analytical solutions in the appropriate domains.

#### 4. Modeling VEX data

In this section we apply the model to the VEX data observed on Dec. 3. 2008, and Nov. 5, 2011 reported in the sections above. Our objective is to interpret the observed heavy ion spectra. The input data of the code are the densities, beam and the thermal velocities of the shocked solar wind protons and planetary ions, the peak magnetic field at the magnetic barrier, and the plasma betas both of the ions and the electron fluid.

The input data cannot be derived from the measurements directly because what we see are the evolved populations, theoretical considerations are also required. The reason is also the coarse time and spatial resolution of the interaction region; the ICB and the IP cannot be really resolved (therefore we shall denote the region as ICB/IP). Our model has been developed for the near IP region; we assume that the shocked solar wind density and the heavy ion density leaked through the IP boundary are equal (5).

The temperature of planetary ions was taken to be 0.1 eV in accordance with the analysis presented in (32). Fluid electron density at the IP was taken to be 100/cc for the average case, in accordance with the density value at the „Brace-ionopause” (33). For the 2011 event we assumed a twice as large value. For the shocked SW velocity and temperature we used the values given above previously. Conditions of quasineutrality  $n_e = n_p + n_i$  and the zero net current in the flow ( $x$ ) direction  $u_e = n_p u_p/n = 1/2 u_p$  are imposed. Fluid electron temperature was 0.2 eV. In reality there are two electron components, a warmer SW and a colder planetary ion component, but it is beyond the reach of the model to take it into account. As discussed above, in the magnetosheath the quality of the input data might be poor due to view conditions, and the spatial resolution as shown in Figures 1 and 2 is sparse (e.g. during 192s the spacecraft altitude changed by about 300

km). This introduces uncertainties into the initial parameters which are carried over to

the output. Therefore the model can reveal tendencies only.

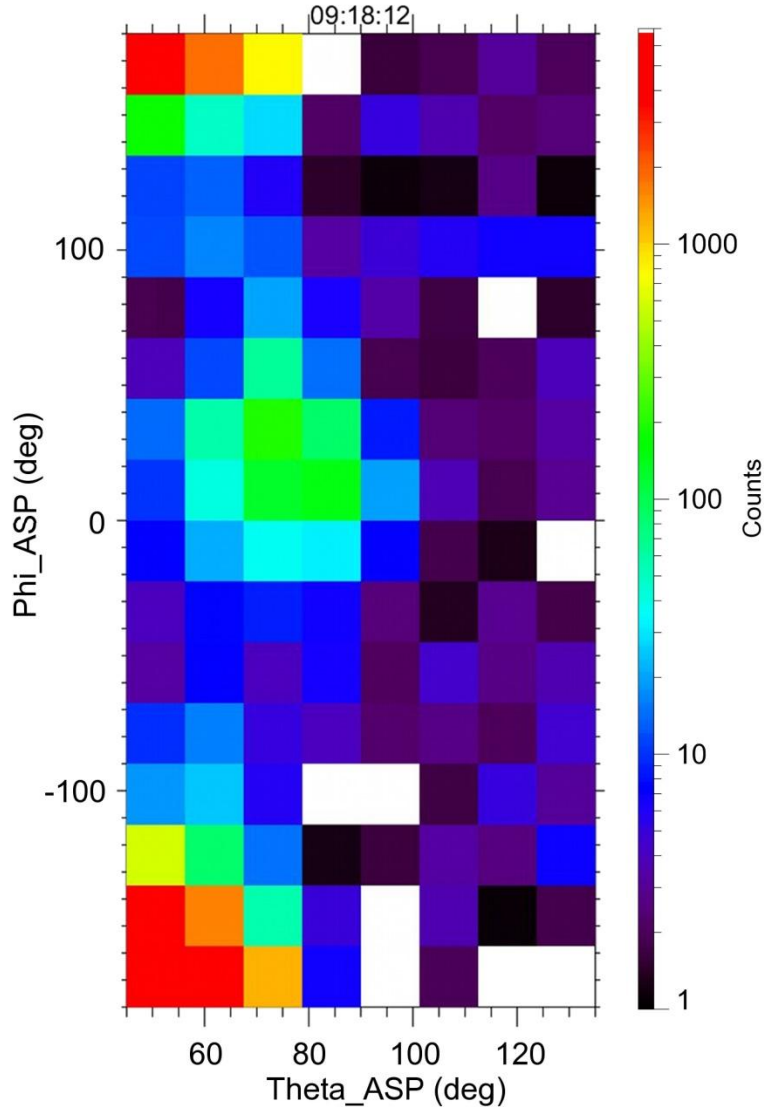


**Figure 6a.** Azimuth –elevation plots (vertical/ horizontal axis) of heavy ions measured during one 192-s long measurement cycle at the ICB for the 2008 case in the spacecraft frame of reference. The counts are summed over the energy channels. The sensor in azimuth is cylindrical, so counts at  $180^\circ$  azimuth „continues” at  $-180^\circ$  azimuth. In VSO, the spacecraft axes at 2008-12-03T09:18:00 were

x-axis: 0.291781, -0.956464, 0.00394974;  
 y-axis: -0.000357644, -0.00423853, -0.999977;  
 z-axis: 0.956485, 0.291772, -0.00157880.

the azimuth being measured from the x axis of the spacecraft; the elevation (Theta) is measured from the x-z plane, positive in y-direction; the y axis is the direction about which the FOV is 360 degree. At the time of the measurement the spacecraft z-axis pointed roughly towards VSO-x, being positive Sunward.

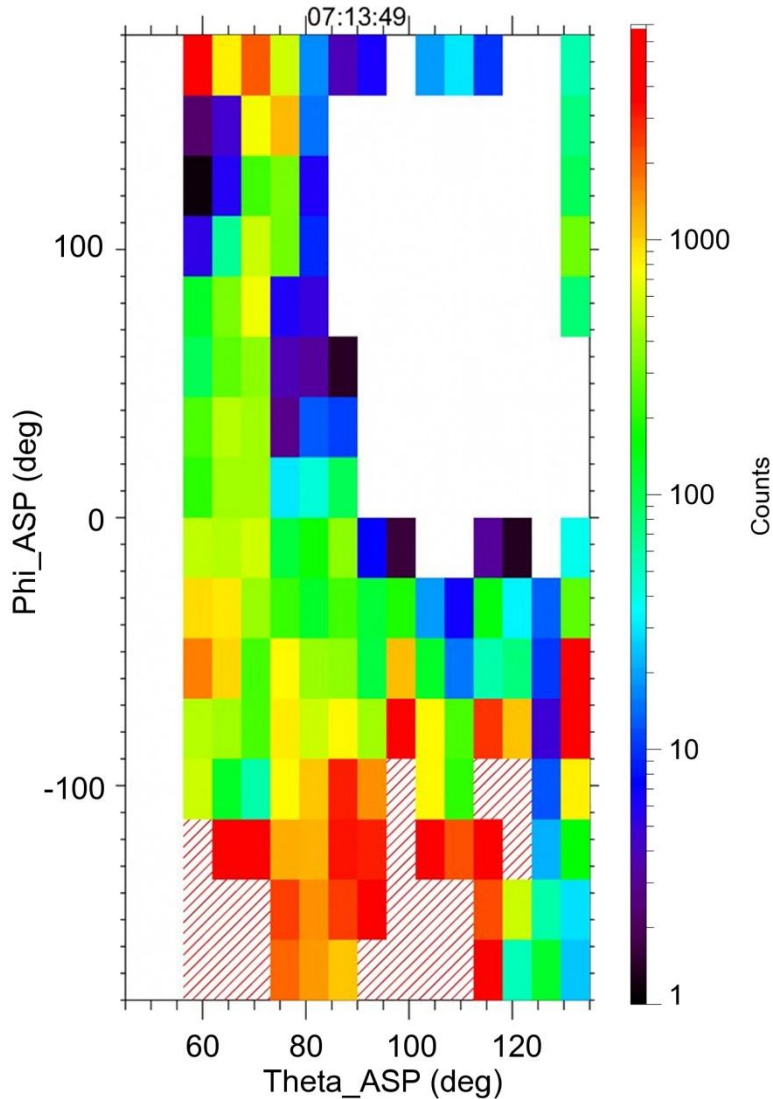


**Figure 6b.** Same as Figure 6a for 2011-11-03T07:13. The spacecraft axes in VSO were:

x-axis: 1.00000, -0.000491881, 1.99527e-005;  
 y-axis: -0.000491892, -0.999991, 0.000283616;  
 z-axis: 1.98133e-005, -0.000283625, -0.999991

The shocked solar wind bulk and thermal speed are measured in 192s steps, and were given in the sections above, based partially on the preliminary ion moments accessible in the AMDA database [<http://amda.cdpp.eu/>], and on the results presented in Fig. 3. The initial heavy ion velocity was taken to be zero, though in reality ions move towards the nightside with

a few km/s velocity due to the ion transport from dayside to nightside (34).

The simulations the box contained 30,000 ions and protons, time and distance were measured in normalized units,  $t \omega_{LH}$ , and  $(1/\omega_{ce}) (T_p/m_e)^{1/2}$ . Velocities in the  $x$  direction are normalized to the proton thermal velocity. The simulations were run till non-linear saturation was reached.

Energy and momentum conservation was better than 1%. The presence of well-developed vortices in the phase space of protons suggests that saturation of the instability takes place via electrostatic trapping. The length of the box was selected to contain at least 5 waves. In physical units for case 1 (case 2) the length of the simulation box is 440m (~100 m), the time needed to reach saturation ( $\omega_{LH}=19.54$  Hz, 195 Hz, resp.) is ~15 s (1.5s). This is surprisingly short time and short length; on one hand it shows that the MTSI interaction is a very effective mechanism, on the other hand it is also due to the periodic boundary condition applied in the present 1-D model (i.e. particles already perturbed by the instability after leaving the simulation box at one end re-enter the simulation box at the other end with unchanged velocities). The question naturally arises why this excitation mode is not dominant everywhere. The answer lies in the dependence of the growth rate on the angle between the wave vector and  $B_0$ . The excitation is effective only when this angle is close to 90 degrees. This angle is reached only near the induced magnetosphere boundary where the field is draping. Further details of the simulation can be found in (23), and in D2005 and D2007.

The present simulation makes possible to calculate the 1-d distribution functions and the moments. In Figures 3a and 3b we display the distribution functions of planetary ions in velocity space after reaching saturation, velocities are normalized to  $v_{Tp}$ , densities to  $n_p$ . The strong heating is evident. In Figures 4a and 4b we show the time development of the bulk and random energy of the SW protons and planetary ions, respectively; that is the energy redistribution of the initial free energy carried by the protons. Data values are normalized to the proton kinetic energy. In Figure. 4a (case 2008) the bulk proton energy drops to ~20% of its initial value;

whereas the random proton energy (~temperature) increases almost 6 times. The random energy of the planetary ions reaches about ~2/3 of the proton random energy (in absolute unit ~125 eV). Till the end of the simulation the bulk speed of the shocked solar wind protons (not shown) drops to ~50% of the initial value, the oxygen ions gain a small speed. The first momentum of the distribution functions shown in Figures 3a and 3b, a bulk speed of the order of ~900 m/s is obtained.

In Figure 4b (case 2011) the bulk proton energy drops to ~30% of its initial value; whereas the random proton energy (~temperature) increases almost 3.5 times. The random energy of the planetary ions reaches about ~60% of the proton random energy (in absolute unit ~400 eV). Till the end of the simulation the bulk speed of the shocked solar wind protons (not shown) drops to ~54% of the initial value, the oxygen ions gain a small speed, of about 3-5% of the initial proton speed (~10 km/s).

## 5. Discussion of simulation results and conclusions

The focal question of this paper is how we can interpret the observed heavy ion heating in the ion composition boundary layer. Especially, we have investigated whether the modified two stream instability excited in the boundary layer may explain the observed heavy ion energy spectra. The measured and the modeled energy spectra in the boundary layer are shown in Figure 5. In Figure 6 we exhibit the measured angular distributions; as the model is 1d, these evidently have no model comparison. The angular distributions shown are the measured ones in the spacecraft frame of reference. Without going into the details, the 2008 plot exhibits that the distribution has two distinct portions; the high density part is basically at rest in VSO, the lower density

peak moves sunward. For 2011 the angular plot does not reveal specific directions. As shown in (12), in the tail region the bulk motion of heavy ions is frequently sunward due to large scale turbulences. In Figure 6a the angular distribution of the heavy ions are shown in the boundary layer forming two distinct populations of the cold ionospheric ions and its tail. The bulk motion of the tail particles flows towards Venus (similar to the results of (12), the gap – we believe – is due to the changing velocity direction, in the gap the flow speed is outside of the instrument field of view. This speed is much higher what the simulation can yield. The unknown spacecraft potential might also contribute to that.

In Figures 5, the simulated phase space densities (denoted by crosses) as function of energy are overplotted on the experimental phase space densities (continuous line). The horizontal axis is energy in eV, the vertical axis is phase space density in  $s \text{ km}^{-2}$ . The continuous lines are the measured values; the crosses denote the results of the simulation. The blue curves are Maxwellian fits. The energy spectra shown in Figure 5 are more extended in energy than the model; the lower energy part is fitted quite well. We believe that the discrepancy in the high energy part is due to model limitations, see below. However, solar wind forcing (10,13) is also might be in operation, forcing the ions to move tailward creating the high energy tail. We believe that the data gap seen in the 2008 measurements are due to large scale turbulences, making the flow to move outside the instrument field of view. Here we focus on the random motion (heating), with the aim to understand its details.

The simulated MTSI heating extends to low energy up to their high energy tail. It is evident from the plots that the ion tail near and above 1000 eV cannot be accounted for by MTSI. Had we run the simulation much further in time, we could have violated the

“unmagnetized ions” condition. As we have emphasized above, the model shows tendencies rather than exact values. We believe that the discrepancy at higher energies (between few hundreds eV – 1 keV) between the model and the data are due to the limitations of the model; its 1-d nature and the fact that we cannot run it in the saturated regime, as explained above. The heating contributed by the simulation compared to the data in our opinion indicate that the MTSI mechanism is in the right ballpark even if many details are imperfect.

The model we have presented is one-dimensional. The reason behind it, let alone the complexity of any multidimensional approach, is the spatial resolution required. The model, since it retains electron inertia, has to resolve electron gyroradius; and this does not allow a large modelling volume taking into account computational needs. However, for computable volumes it is difficult to set boundary conditions, because they would be much arbitrary with the current data resolution in the sheath. The one-dimensionality on the other hand restricts the spread of energy in directions perpendicular to the flow, probably affecting energy redistribution between the particle components. This is a difficulty we have to live with. The model results account for the energy redistribution due to MTSI between protons and heavy ions, concerning bulk and random energy.

To overcome the limitations of the 1-d simulation model with periodic boundary conditions we need to use non-periodic boundary conditions so that a constant injection of the solar-wind protons and refurbishing of the cold ionospheric ions in the simulation box can take place, and the instability will be saturated in distance, not in time. Inclusion of electron particle effects, such as Landau damping, should also be studied. This will necessitate the use of the particle simulation codes for electrons.

Finally, the model should be extended to multiple spatial dimensions with non-periodic boundary conditions to be able to examine the effect of the finite height of the interaction region as well as the wave spectral modifications introduced by the observed shear in the magnetic field.

It was mentioned above (and shown in Figures 1 and 2) that during one measurement cycle the spacecraft altitude may change more than 300 km. Between ICB/IP therefore different populations may mix, the decelerating shocked solar wind and flow under the influence of MTSI.

In summary, the heating what the MTSI mechanism provides might be an

essential contribution to the heating of heavy ions near the ICB, even if the match is not perfect. MTSI does not explain the observed ion velocities. We believe that the observed heavy ion heating proves that the MTSI mechanism is operating near the ICB, but certainly it is not the only mechanism required to interpret the data.

### **Acknowledgement**

Part of data analysis was performed with the AMDA science analysis system provided by the Centre de Données de la Physique des Plasmas (CDPP) supported by CNRS, CNES, Observatoire de Paris and Université Paul Sabatier, Toulouse.

## References

1. K Spenner, WC Knudsen, KL Miller, V Novak, CT Russel, and RC Elphic, (1980), Observation of the Venus mantle, boundary region between solar wind and ionosphere, *J. Geophys. Res.*, 85, 7655–7662.
2. A Coates et al., (2008), Ionospheric photoelectrons at Venus: Initial observations by ASPERA-4 ELS, *Planetary and Space Science* 56, 802–806.
3. TL Zhang, JG Luhmann, and CT Russell (1991), The magnetic barrier at Venus, *J. Geophys. Res.*, 96, 11,145–11,153.
4. RJ Strangeway, and CT. Russell, Plasma waves and field aligned currents in the Venus plasma mantle, (1996), *J. Geophys. Res.*, **101**, 17,313.
5. VD Shapiro, K. Szego, SK. Ride, AF Nagy, and VI Shevchenko (1995), On the interaction between the shocked solar wind and the planetary ions in the dayside of Venus, *J. Geophys. Res.*, 100, 21,289 – 21,298.
6. JM Grebowsky, WT Kasprzak, RE Hartle, KK Majahan, and TCG Wagner, (1993), Superthermal ions detected in Venus' dayside ionosheath, ionopause and magnetic barrier regions, *J. Geophys. Res.*, 98, 9055.
7. DS Intriligator, JH Wolfe, and JD Mihalov (1980), The Pioneer Venus Orbiter plasma analyzer experiment, *IEEE Trans. Geosci. Remote Sens.*, GE-18, 39–43, doi:10.1109/TGRS.1980.350258.
8. S Barabash et al., (2007) The loss of ions through the plasma wake, *Nature*. 450, pp. 650-653, doi:10.1038/nature06434
9. C Martinecz et al. [2008] *Planetary and Space Science* 56 (2008) 780–784, doi:10.1016/j.pss.2007.07.007
10. R Lundin, (2011), Ion acceleration and outflow from Mars and Venus, an overview, *Space Sci. Rev.*, 162, 309
11. C Bertucci, F Duru, N Edberg, M Fraenz, C Martinecz, K Szego, O Vaisberg, The Induced Magnetospheres of Mars, Venus, and Titan, *Space Sci. Rev.*, 2011,162, 113–171.
12. A Fedorov, S Barabash, JA Sauvaud, Y Futaana, TL Zhang, R Lundin, and C Ferrier (2011), Measurements of the ion escape rates from Venus for solar minimum, *J. Geophys. Res.*, 116, A07220, doi:10.1029/2011JA016427
13. E Dubinin, M Fraenz, A Fedorov, R Lundin, N Edberg, F Duru, O Vaisberg, (2011), Ion Energization and Escape on Mars and Venus, *Space Sci. Rev.*, 162, 173.
14. TL Zhang, et al. (2006), Magnetic field investigation of the Venus plasma environment: Expected new results, *Planet. Space Sci.*, 54, 1336–1343, doi:10.1016/j.pss.2006.04.018.
15. S Barabash, et al. (2007a), The Analyser of Space Plasmas and Energetic Atoms (ASPERA-4) for the Venus Express mission, *Planet. Space Sci.*, 55, 1772–1792, doi:10.1016/j.pss.2007.01.014.
16. LH Brace, RF Theis, WR Hoegy, Plasma clouds above the ionopause of Venus and their implications. (1982) *Planet. Space Sci.* 30, 29–37, doi:10.1016/j.pss.2007.12.08

17. RJ Strangeway, (1991), Plasma Waves At Venus, *Space Science Reviews* 55: 275-316.
18. FL Scarf, WL Taylor, CT Russell, and RC Elphic, (1980), Pioneer Venus plasma wave observations: The solar wind-Venus interaction, *J. Geophys. Res.*, 8, 7599.
19. RZ Sagdeev, *et al.*, (1990), Wave activity in the neighborhood of the bowshock of Mars, *Geophys. Res. Lett.* **17**, 893-896, doi:10.1029/GL017i006p00893
20. JD Huba, (1993), Generation of waves in the Venus mantle by the ion acoustic beam instability, *Geophys. Res. Lett.* **20**, 1751
21. K Szego, VS Shapiro, VI Shevchenko, RZ Sagdeev, WT Kasprzak, AF Nagy, (1991), Physical processes in the plasma mantle of Venus, *Geophysical Research Letters*, 18, 2305-2308
22. KB Quest, VD Shapiro, K Szego, and Z Dobe, (1997), Microphysics of the Venusian and Martian mantles, *Geophys. Res. Lett.*, 24, 301– 304.
23. Z Dobe, KB Quest, VD Shapiro, K Szego, and JD Huba (1999), Interaction of the solar wind with unmagnetized planets, *Phys. Rev. Lett.*, 83, 260–263.
24. K Szego, Z Dobe, J Huba, K Quest, and VD Shapiro, (2000), Wave activity in the dayside mantle of Venus, Mars, and Titan, *Adv. Space Res.*, 26, 1609–1612.
25. Z Dobe, and K Szego (2005), Wave activity above the ionosphere of Titan: Predictions for the Cassini mission, 27 *J. Geophys. Res.*, 110, A03224, doi:10.1029/2004JA010548.
26. CS Wu, YM Zhou, ST Tsai, SG Guo, D Winske, and K Papadopoulos (1983), A kinetic cross-field streaming instability, *Phys. Fluids*, 26, 1259–1267.
27. SP Gary, and N Omid (1987), The ion/ion acoustic instability, *J. Plasma Phys.*, 37, 45–61.
28. Z Dobe, K Szego, KB Quest, VD Shapiro, RE Hartle, and EC Sittler Jr. (2007), Nonlinear evolution of modified two-stream instability above ionosphere of Titan: Comparison with the data of the Cassini Plasma Spectrometer, *J. Geophys. Res.*, 112, A03203, doi:10.1029/2006JA011770.
29. SH Brecht, JG Luhmann, and DJ Larson (2000), Simulation of the Saturnine magnetospheric interaction with Titan, *J. Geophys. Res.*, 105, 13,119– 13,130
30. E Kallio, L Sillanpaa, and P Janhunnen (2004), Titan's subsonic and supersonic flow, *Geophys. Res. Lett.*, 31, L15703, doi:10.1029/2004GL020344.
31. SA Ledvina, and TE Cravens (1998), A three-dimensional MHD model of plasma flow around Titan, *Planet. Space Sci.*, 46, 1175– 1192.
32. KL Miller, and RC Whitten, (1991), Ion dynamics in the Venus ionosphere, *Space Science Reviews*, 55; 165-199.
33. LH Brace, and AJ Kliore, (1991), The structure of the Venus ionosphere, *Space Science Reviews* 55: 81-163.
34. WC Knudsen, PM Banks, and KL Miller, (1982), A Model of Plasma Motion and Planetary Magnetic Fields for Venus, *Geophys. Res. Letters* 9, 765.